



Full Length Article

Achieving bi-lamellar microstructure with both high tensile strength and large ductility in Ti–6Al–4V alloy by novel thermomechanical processing

Yan Chong ^{a,b,*}, Tilak Bhattacharjee ^{a,c}, Jangho Yi ^a, Shiteng Zhao ^{a,b}, Nobuhiro Tsuji ^{a,c}^a Department of Materials Science and Engineering, Kyoto University, Kyoto, Japan^b Department of Materials Science and Engineering, University of California, Berkeley, USA^c Elements Strategy Initiative for Structural Materials (ESISIM), Kyoto University, Kyoto, Japan

ARTICLE INFO

Keywords:
 Ti–6Al–4V
 Lamellar
 Bi-lamellar
 Colony size
 Micro-shear bands

ABSTRACT

In this study, a novel through- β -transus processing followed by intercritical annealing was designed to obtain the bi-lamellar microstructure in Ti–6Al–4V alloy with refined colony sizes, by which both tensile strength and ductility were significantly improved. The colony size obtained in the through- β -transus processing was 60 μm , much smaller than the minimum colony size of 130 μm that can be achieved in the conventional β processing. The colony refinement was attributed to the decreased size of the grain boundary α phase with increased variety of crystallographic orientations, which acted as nucleation sites for subsequent colony structures. By intercritical annealing of the lamellar microstructures in $\alpha+\beta$ two-phase region followed by water quenching, bi-lamellar microstructures composed of primary α lamellae and transformed β regions composed of fine secondary α plates were obtained, maintaining the same colony size as the lamellar precursors. The total elongation of bi-lamellar microstructure significantly improved from 3.4% to 18.6% with decreasing the colony size, while the high yield and tensile strength was independent of the colony size. SEM-EBSD characterization of the bi-lamellar microstructures at interrupted tensile strains clarified that deformation behaviors of the bi-lamellar microstructures after yielding were mainly controlled by micro-shear bands across transformed β regions, which eventually evolved into micro-cracks at higher tensile strains. It was considered that the strain compatibility accommodated by the differently aligned micro-shear bands formed within different colonies was the main reason for delaying tensile fracture in the bi-lamellar microstructure with the smaller colony size.

1. Introduction

Ti–6Al–4V alloy comprised of hexagonal close packed (HCP) α phase and body-centered cubic (BCC) β phase has been widely used in aerospace, biomedical and petroleum industries, because of the high specific strength, moderate ductility, good biocompatibility and high corrosion resistance, [1]. Depending on thermomechanical processing histories, four kinds of typical microstructures, i.e., lamellar microstructure, martensite microstructure, bimodal microstructure and equiaxed microstructure are obtained in Ti–6Al–4V alloy. Lutjering [2,3] has discussed the relationship between thermomechanical processing parameters and resulting microstructures as well as their mechanical properties in Ti–6Al–4V alloy. When the alloy was cooled from β single-phase region, lamellar or martensite microstructure forms depending on the cooling rate. In reality, it is difficult to get a fully martensite microstructure in the alloy due to a requirement of fast cooling rate and low thermal conductivity of Ti, which makes the lamellar microstructure more popular in industries. The lamellar microstructure is characterized

by high fracture toughness and good creep strength, but its moderate strength and ductility limits wider industrial applications [2,3]. The equiaxed or bimodal microstructures show better balance of strength and ductility, but in practice, hot deformation in $\alpha+\beta$ two-phase region has to be applied for obtaining those microstructures in order to break α lamellae to make equiaxed α [4–8]. This process, termed as globularization, is the most difficult step from a workability standpoint. Therefore, any way to simultaneously increase the strength and ductility of lamellar-based microstructures without hot deformation in $\alpha+\beta$ two-phase region would reduce the cost of Ti–6Al–4V product.

In the β to α phase transformation, the Burgers orientation relationship, $\{0001\}_{\alpha} // \{110\}_{\beta}$, $<11-20>_{\alpha} // <111>_{\beta}$, is satisfied between two phases [9], rendering 12 possible variants of α lamellae formed from a single β grain. The α lamellae having the same crystallographic variant make up a colony, and α lamellae belonging to different colonies have different crystallographic orientations. It is believed that the effective slip length in the plastic deformation at room temperature is provided by the colony size in lamellar microstructures, as interphase

* Corresponding author at: Department of Materials Science and Engineering, University of California, Berkeley, USA.

E-mail address: chongyan@berkeley.edu (Y. Chong).

boundaries between α lamellae and retained β within an identical colony is semi-coherent showing little resistance to dislocation glide [10–16]. Therefore, a smaller colony size is always desirable for better mechanical properties, i.e., higher strength and better creep properties. Increasing the cooling rate after β annealing has been frequently used to refine the colony size and the thickness of α lamellae [5,7]. However, when the cooling rate exceeds some critical value, so-called basketweave or martensite microstructures form, both of which are characterized by fine α (or α') lamellae with various orientations. In these microstructures, each α/α' lamella is surrounded by other α/α' lamellae having different orientations and directions, so that there are substantially no colonies in these two microstructures. As a result, the mechanical behaviors of basketweave and martensite microstructures significantly differ from those of the lamellar microstructure. It should be also noted that, due to the requirement of fast cooling rate and lower thermal conductivity in Ti, it is almost impossible to get a fully martensite microstructure throughout the whole components, especially for those with large cross sections. Resultant microstructure gradient from the surface to the center would be undesirable for industrial applications.

In addition to the colony refinement, an alternative way to reduce the effective slip length in the microstructures based on α lamellae is to introduce secondary α lamellae transformed from β regions between coarse α lamellae, which is so-called bi-lamellar microstructure termed by Lutjering [2,3,17]. In intercritical annealing of lamellar microstructures in $\alpha+\beta$ two-phase region, thickness and volume fraction of retained β existing between α lamellae increase, and the β regions again transformed into fine secondary α lamellae (including small amounts of retained β) during subsequent quenching. The effective slip length is significantly reduced in the bi-lamellar microstructure compared with that in the lamellar microstructure. It has been proved that the bi-lamellar microstructure is beneficial for most mechanical properties, including tensile, fatigue and creep strength [2,3]. However, the bi-lamellar microstructure has not attracted much attention and systematic investigations concerning the effect of initial colony size on the mechanical properties of bi-lamellar microstructures have not been fully understood yet.

In this study, different thermomechanical processes are applied to Ti-6Al-4V alloy for refining the colony size of both lamellar and bi-lamellar microstructures. Then, the mechanical properties of both microstructures with different colony sizes are evaluated at room temperature. Finally, the mechanisms of colony refinement as well as its influence on mechanical properties and deformation behaviors of both microstructures are discussed in detail.

2. Experimental procedure

Ti-6Al-4V alloy with a detailed chemical composition of Ti-6.29Al-4.35V-0.155O-0.225Fe-0.105C-0.085N (wt%) was used in this study. The β transus temperature ($T_{\beta\text{trans}}$) of the used alloy was determined to be $\sim 983^\circ\text{C}$ by a metallographical method. Initial microstructure of the as-received material was a lamellar microstructure with an average colony size of $\sim 300\ \mu\text{m}$. Cylindrical samples with a diameter of 10 mm and height of 15 mm were cut from the as-received billet for subsequent thermomechanical processing. Two types of thermomechanical processes (Fig. 1(a) and (b)) was carried out using a thermomechanical processing simulator (Thermecmaster-Z). In the first type (Fig. 1(a)), the samples were uniaxially compressed at 1040°C (β single-phase region) at a strain rate of $0.01\ \text{s}^{-1}$ to different true strains of 0–1.5, followed by slow cooling ($50\ ^\circ\text{C}\ \text{min}^{-1}$) to room temperature. This is termed as the β processing method hereafter. In the second type (Fig. 1(b)), the samples were uniaxially compressed at 1040°C at a strain rate of $0.01\ \text{s}^{-1}$ to a true strain of 0.6, followed by slow cooling ($50\ ^\circ\text{C}\ \text{min}^{-1}$) to room temperature. During the early stage of cooling (from 1040°C to 940°C), the samples were concurrently compressed at a strain rate of $0.005\ \text{s}^{-1}$ to a true strain of 0.6. The total true strain applied was 1.2 in this second process. This is termed as the through- β -transus processing method here-

after. After both thermomechanical processing methods, intercritical annealing was carried out at 910°C ($\alpha+\beta$ two-phase region) for 20 min followed by water quenching (Fig. 1(c)), which was designed to transform the lamellar microstructures into bi-lamellar microstructures.

After the thermomechanical processing or intercritical annealing, the samples were cut in half along a diameter of the cylinder. The sections parallel to the compression axis were then ground and polished, following standard metallographical methods. After mechanical polishing using 4000# SiC sand paper, the samples were subsequently electro-polished in a solution of 10% perchloric acid and 90% methanol at -30°C for 30 s. Microstructural characterization was carried out at the center on the sections described above. Backscattered electron (BSE) observations were conducted using a JEOL 7800F scanning electron microscope (SEM) operated at an accelerating voltage of 15 kV. Electron backscattered diffraction (EBSD) investigations were conducted using the TSL system attached to a field emission gun SEM (JEOL 7100F) operated at an accelerating voltage of 15 kV. The step size of the EBSD scan was $0.04\ \mu\text{m}$. The collected data were analyzed using the TSL-OIM software. Boundaries with misorientation angles of $2\text{--}15^\circ$ and those higher than 15° were defined as LAGBs and HAGBs, respectively. The length density of HAGBs (ρ_{HAGB}) was calculated by dividing the total length of HAGBs (given by the OIM software) by the area of the scanned region. For slip line and micro-shear band analysis, pre-polished surfaces of tensile specimens were directly observed by EBSD after a tensile deformation. Slip traces inside primary α lamellae were crystallographically analyzed by the OIM software. Specimens for transmission electron microscopy (TEM) were prepared by a standard twin-jet electro-polishing technique using a Struers TenuPol-5 device. Slices of $0.3\ \mu\text{m}$ thickness were cut from thermomechanically processed samples, mechanically ground to $40\text{--}50\ \mu\text{m}$ in thickness, and then electro-polished at -40°C at a voltage of 20 V in a solution containing 90% methanol and 10% perchloric acid. TEM investigations were conducted using JEOL 2010 TEM operated at 200 kV.

Micro-tensile specimens with a gauge length of 3.0 mm, width of 1.5 mm and thickness of 0.8 mm were cut from the center of the thermomechanical processed or intercritical annealed samples. The broad face of the sheet-type tensile specimen was parallel to the compression axis, and the tensile direction of the specimen was perpendicular to the compression axis. Tensile tests were conducted on Shimadzu AG-X plus system at room temperature at an initial strain rate of $8.3 \times 10^{-4}\ \text{s}^{-1}$. It has been confirmed in our previous studies that the micro-tensile specimen can give reliable stress-strain data equivalent to those obtained from standard-sized specimen of the same material [18]. The deformation strains of the micro-tensile specimens were precisely measured by the digital image correlation (DIC) method. The details of the DIC method can be found elsewhere [19]. For each condition, at least three specimens were tested, and the average values of mechanical properties were used in this study.

3. Results

3.1. Colony refinement by thermomechanical processing

In the β processing method, different compression strains ($\varepsilon = 0, 0.3, 0.6, 0.9, 1.2$ and 1.5) were applied. Obtained grain boundary maps of the β processed microstructures corresponding to different compression strains are shown in Fig. 2, in which blue and red lines represent HAGBs and LAGBs, respectively. Since misorientation angles between different colonies in the lamellar microstructures were larger than 15° in general, each area surrounded by HAGBs was considered as a colony in this study for simplicity. In the undeformed microstructure (Fig. 2(a)), the coarse colony structure was observed, which was typical in Ti-6Al-4V alloy after β annealing [3,5,7]. In the β processed microstructures (Fig. 2(b)–(f)), however, colony sizes were in general much smaller than that in (a). In order to quantify the colony size, the equivalent colony size (D_e) was defined as $D_e = 2/\rho_{\text{HAGB}}$, in which ρ_{HAGB} was the length density of HAGBs

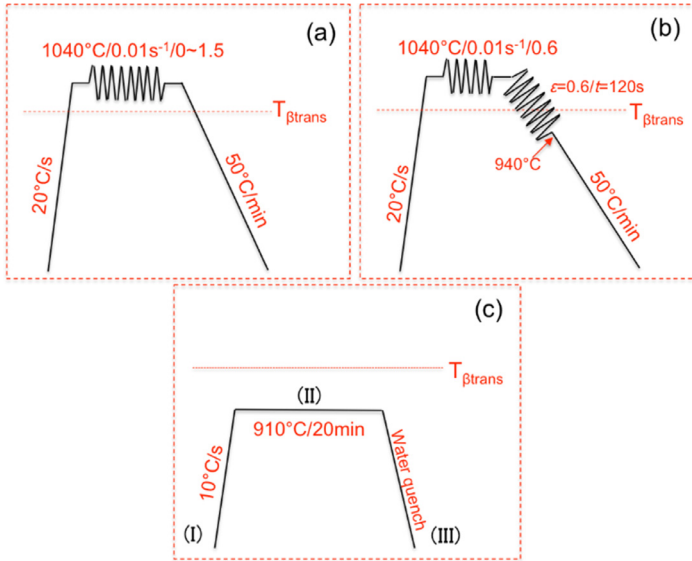


Fig. 1. Schematic illustrations showing the β processing method (a), the through- β -transus processing method (b) and the subsequent intercritical annealing treatment (c).

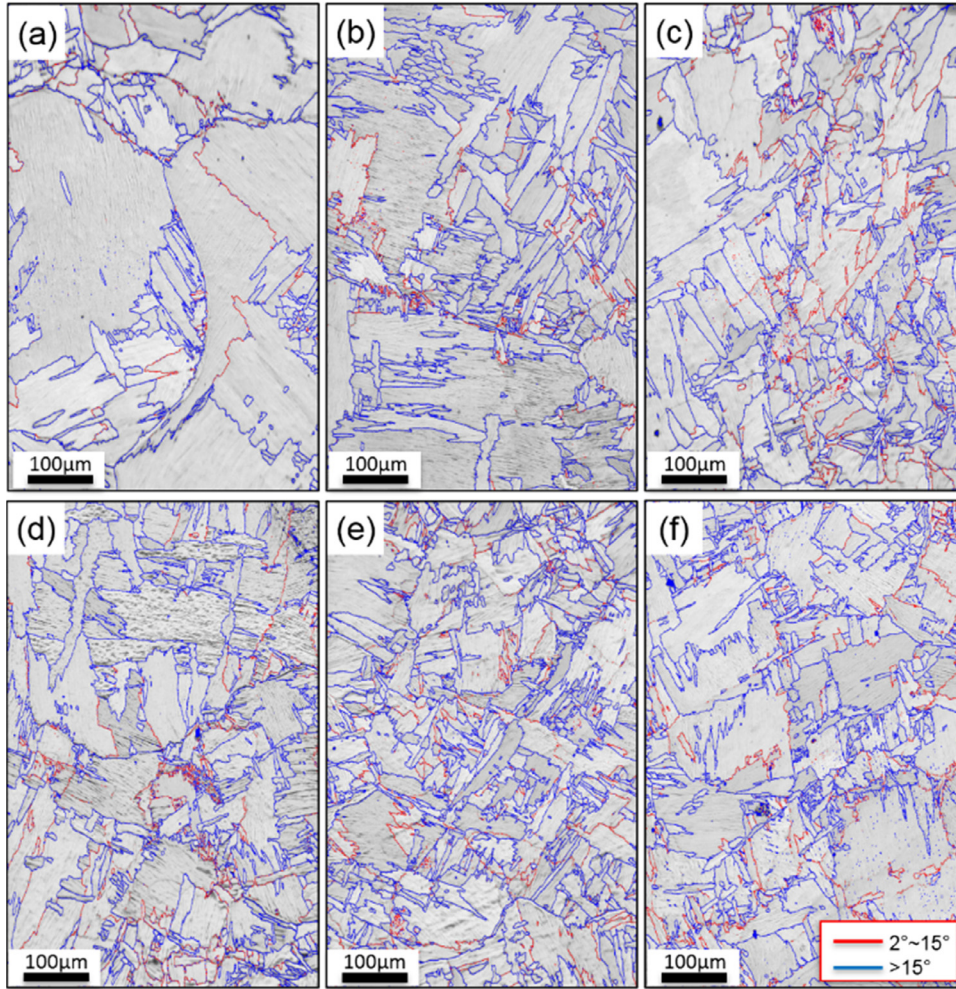


Fig. 2. EBSD grain boundary maps of β processed microstructures with different compression strains (ϵ): (a) $\epsilon=0$; (b) $\epsilon=0.3$; (c) $\epsilon=0.6$; (d) $\epsilon=0.9$; (e) $\epsilon=1.2$ and (f) $\epsilon=1.5$. Blue and red lines represent HAGBs and LAGBs, respectively. The compression axis is parallel to the longitudinal directions of the figures for all microstructures.

described in the former section. The calculated D_e and ρ_{HAGB} were plotted against the compression strain (Fig. 3). It clearly showed that the equivalent colony size quickly decreased from $\sim 280 \mu\text{m}$ in the undeformed microstructure to $\sim 180 \mu\text{m}$ in the β processed microstructure deformed by a compression strain of 0.3. With increasing the compression strain, the equivalent colony size furthermore decreased, and the

minimum colony size of $\sim 130 \mu\text{m}$ was obtained in the sample deformed to a compression strain of 1.2. The refinement of colony saturated over 1.2 of strain.

In order to furthermore refine the colony size, the through- β -transus processing was designed (Fig. 1(b)), in which the sample was deformed not only in the β single-phase region (1040 °C), but also during the early

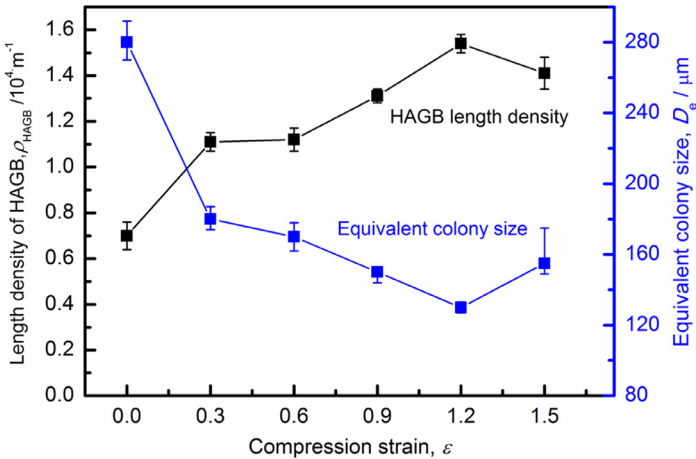


Fig. 3. Change of the HAGB length density ρ_{HAGB} (total length of HAGBs divided by area of observation) and the equivalent colony size D_e ($2/\rho_{\text{HAGB}}$) with compression strain in the β processed microstructures.

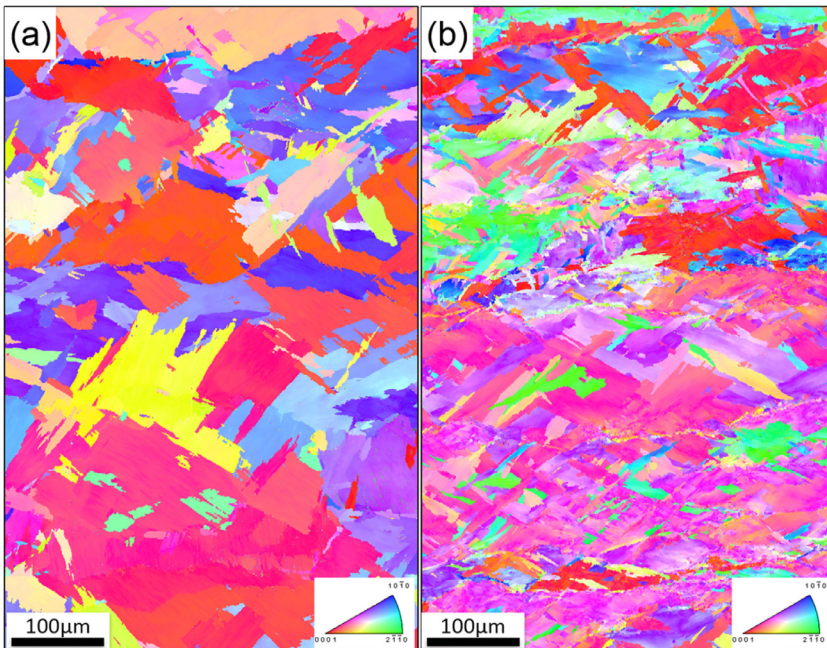


Fig. 4. EBSD IPF maps of α phase after the β process with a compression strain of 1.2 (a), and after the through- β -transus process with a total compression strain of 1.2 (b). The compression axis is along the longitudinal direction of the figures. The equivalent colony size in the through- β -transus processed microstructure was much smaller than that in the β processed microstructure with the same total compression strain applied.

stage of cooling (from 1040 °C to 940 °C). The total strain applied was 1.2, which was the same as that for the microstructure with the minimum colony size obtained in β processing. The IPF maps of α phase in the β processed microstructure with the minimum colony size ($\epsilon=1.2$) as well as those in the microstructures after the through- β -transus process are shown in Fig. 4(a), and (b), respectively. It was clearly shown that the colony sizes in the through- β -transus processed microstructures became much smaller than that in the β processed microstructure, although the total strain applied was the same in two processes. Using the same method described above, the equivalent colony size in the through- β -transus processed microstructure was calculated to be $\sim 60 \mu\text{m}$, which was less than half of the minimum colony size obtained in the β processed microstructure. Therefore, it can be concluded that the through- β -transus processing method is more effective than the β processing method in refining the colony size of the lamellar microstructure in Ti-6Al-4V alloy.

3.2. Transforming the lamellar microstructure into bi-lamellar microstructure

After obtaining the lamellar microstructures with different colony sizes using either the β processing or the through- β -transus processing described above, an intercritical annealing in $\alpha+\beta$ two-phase re-

gion (910 °C) shown in Fig. 1(c) was carried out to change the lamellar microstructures into bi-lamellar microstructures. The schematic illustration of the microstructure evolution during each step of the intercritical annealing (marked as (I), (II) and (III) in Fig. 1(c)) is shown in Fig. 5(a). Before the intercritical annealing (I), the microstructure was mostly comprised of α lamellae as well as a small amount of β retained between α lamellae. The retained β was quite thin at room temperature. During the intercritical annealing (II), the thickness of retained β increased at the expense of the thickness of α lamellae, and the volume fraction of β increased according to the equilibrium phase diagram. The β phase with increased thickness and volume fraction was not stable during water quenching (III), but would again transform into fine secondary α lamellae having different crystallographic orientations and elongated directions. The resulting microstructure is comprised of the initial α lamellae (referred to as primary α lamellae hereafter) and the collection of fine secondary α lamellae and retained β (referred to as transformed β regions hereafter), which is termed as the bi-lamellar microstructure. It is noteworthy that, the colony size (in the primary α lamellae) in the resulting bi-lamellar microstructure is the same as that of the starting lamellar microstructure. Therefore, bi-lamellar microstructures with different colony sizes could also be realized by intercritically annealing the lamellar microstructures with different colony sizes. A typical example of the bi-lamellar microstructure is

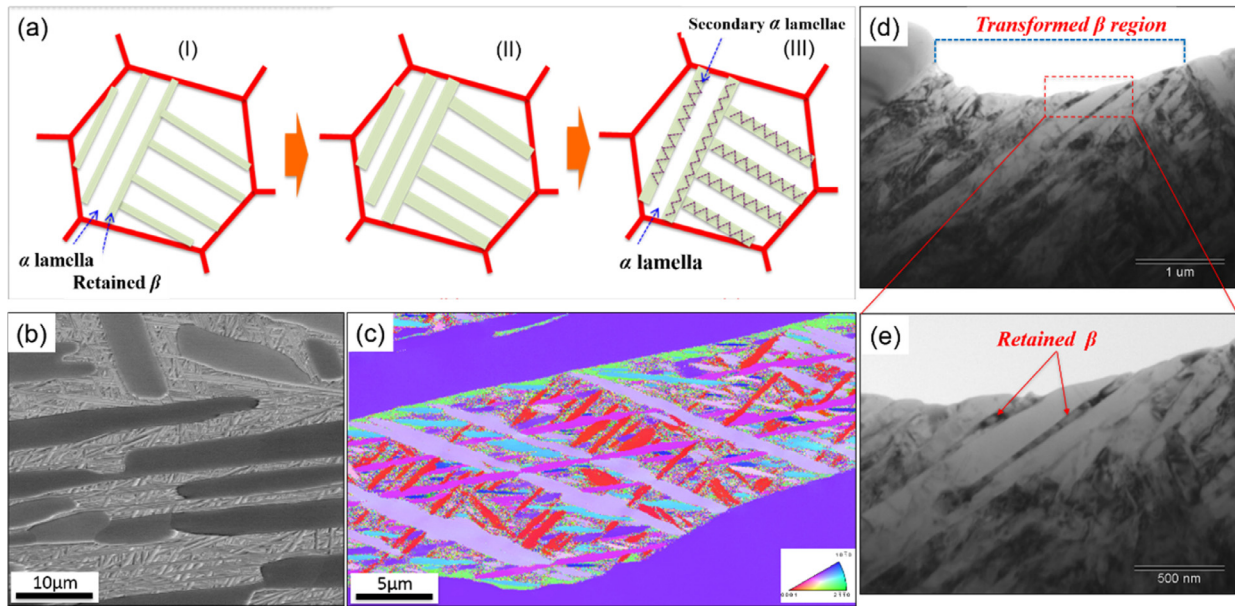


Fig. 5. Bi-lamellar microstructure in Ti-6Al-4V alloy. (a) Schematic illustration of the microstructure evolution during each step of intercritical annealing according to Fig. 1(c). (b) SEM-BSE image of a typical bi-lamellar microstructure obtained by annealing at 910 °C followed by water quenching. (c) EBSD IPF map of α phase in the bi-lamellar microstructure, showing various crystallographic orientations of secondary α lamellae. (d) and (e) TEM images showing a transformed β region (d) and retained β (e) [20].

shown in Fig. 5(b)–(e). Coarse primary α lamellae with an average thickness of about 4 μm and fine secondary α lamellae with an average thickness of about 0.5 μm were clearly shown in the BSE micrograph (Fig. 5(b)). Unlike the primary α lamellae having an identical crystallographic orientation within each colony, the secondary α lamellae generally had various crystallographic orientations (Fig. 5(c)), which was typical for martensite or basketweave microstructures formed in $\alpha+\beta$ titanium alloys after fast quenching. In the TEM images (Fig. 5(d) and (e) [20]), a few retained β phases were also detected in transformed β regions, although the volume fraction of retained β was very small.

3.3. Mechanical properties of lamellar and bi-lamellar microstructures with different colony sizes

After obtaining the lamellar and bi-lamellar microstructures with different colony sizes (ranging from 60 μm to 280 μm), tensile properties of these microstructures were tested at room temperature. Obtained engineering stress-strain curves for both microstructures are shown in Fig. 6(a), where solid and broken lines represent stress-strain curves of the bi-lamellar and the lamellar microstructures, respectively. Corresponding colony sizes are indicated near each curve. The shapes of all these stress-strain curves were similar to each other in general: a continuous decrease in the flow stress shortly after yielding and limited strain hardening. Nevertheless, the bi-lamellar microstructures generally had higher yield and tensile strengths than the lamellar microstructures. In addition, the change of mechanical properties with the colony size was also different between the lamellar and bi-lamellar microstructures (Fig. 6(b)). In the lamellar microstructures, the tensile strength slightly increased with decreasing the colony size, while the total elongation remained almost unchanged. In the bi-lamellar microstructures, on the other hand, the total elongation significantly increased (from 3.4% to 18.6%) with decreasing the colony size, while the high tensile strength ($> 1.0 \text{ GPa}$) was independent of the colony size. In our previous study for bi-lamellar microstructures in Ti-6Al-4V alloy [20], it has been found that the tensile strength of the bi-lamellar microstructure was closely related to the thickness of the transformed β regions, in other words, the intercritical annealing temperature. This explained the nearly identical tensile strength of all the bi-lamellar microstructures obtained after the

same intercritical annealing temperature in the current study, despite of the difference in the colony size. Therefore, it is believed that there are two different scales of microstructural parameters that determine mechanical properties of the bi-lamellar microstructure. The yield and tensile strengths are related to the thickness of the transformed β regions that is determined by the intercritical annealing temperature, as well as the solid solution strengthening by Al in the primary α lamellae [20]. As a result, the maximum yield and tensile strengths of the bi-lamellar microstructures were achieved at an intermediate intercritical annealing temperature [20]. On the other hand, the total elongation of the bi-lamellar microstructure is mainly controlled by the colony size. The larger total elongation is obtained in the microstructures with smaller colony size. It should be emphasized that the bi-lamellar microstructures with finer colony sizes showed much higher strength and larger tensile ductility than the lamellar microstructures with the same colony sizes. The detailed mechanism for the colony size dependence of the total elongation will be discussed in the next section.

4. Discussion

In the last section, we have successfully refined the colony size of both lamellar and bi-lamellar microstructures from 280 μm down to 60 μm , using the β processing and through- β -transus processing. After evaluating tensile properties at room temperature of these microstructures, several interesting phenomena have been found: for example, the much higher yield and tensile strengths of the bi-lamellar microstructures than those of the lamellar microstructures, and the different colony size dependence of mechanical properties between two different microstructures. In this section, we discuss the mechanism of the colony refinement in the applied processes, firstly. Then, detailed deformation mechanisms in the lamellar and bi-lamellar microstructures are discussed, based on which the colony size dependence of the mechanical properties is also explained.

4.1. Mechanism of colony refinement by thermomechanical processing

In previous studies on $\alpha+\beta$ or near β titanium alloys [21–24], it has been confirmed that during cooling after β annealing, α phase firstly

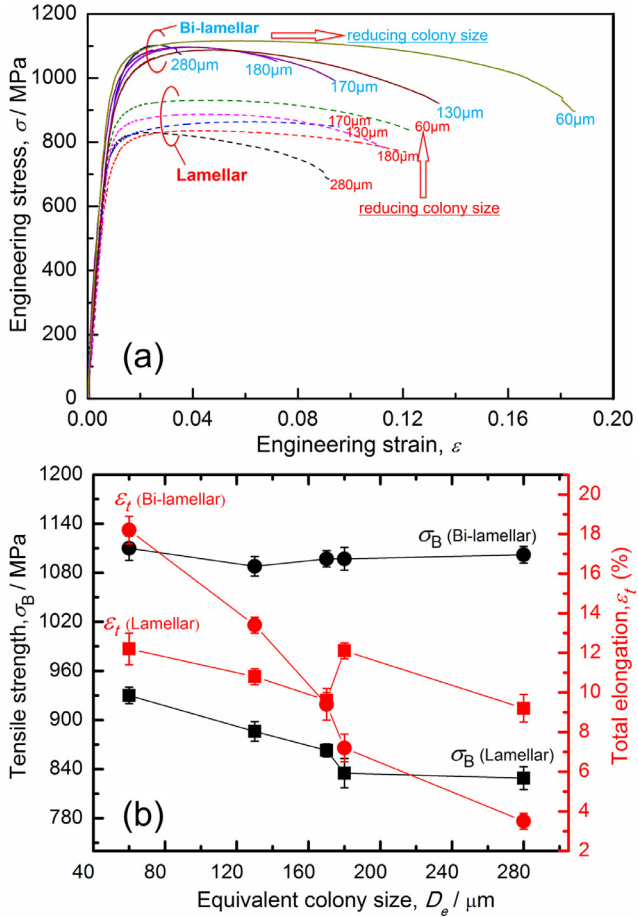


Fig. 6. (a) Engineering stress-strain curves of the lamellar and bi-lamellar microstructures with different colony sizes obtained in Ti–6Al–4V alloy. (b) Tensile strength and total elongation of the lamellar and bi-lamellar microstructures plotted as a function of the colony size. In the lamellar microstructure, the tensile strength gradually increased with decreasing the colony size, while the total elongation was nearly the same. In the bi-lamellar microstructure, on the other hand, the tensile strength was nearly identical for different colony sizes, while the total elongation significantly increased with decreasing the colony size.

forms along grain boundaries of β below β transus temperatures. The grain boundary α phase maintains the Burgers orientation relationship (OR) with one of the β grains facing to the grain boundary. The colony composed of α lamellae having the same crystallographic orientation as adjacent grain boundary α develops in β grains, maintaining the Burgers OR [23]. Growth of the colony stops when it meets other colonies. Therefore, there are two strategies to refine the colony size in lamellar microstructures. The first one is to induce grain boundary α having different crystallographic orientations on each β grain boundary, which act as nucleation sites for the subsequent formation of colony structures. The other one is to reduce the grain size of prior β , and thereby to reduce the colony size inside β grains [25]. In the present study, both β processing and through- β -transus processing methods were designed based on the first strategy. Therefore, detailed EBSD characterization was carried out on three typical microstructures, i.e., the β annealed microstructure plus intercritical annealing ($\varepsilon = 0$) (Fig. 7(a) and (b)), the β processed microstructure with the minimum colony size plus intercritical annealing ($\varepsilon = 1.2$) (Fig. 7(c) and (d)), and the through- β -transus processed microstructure ($\varepsilon = 1.2$) (Fig. 7(e)–(g)), having a particular attention to the crystallographic orientations of grain boundary α phase. EBSD IPF maps of α phase for the three different microstructures are shown in Fig. 7(a), (c) and (e) with corresponding image quality maps as well as grain boundary maps shown in Fig. 7(b), (d) and (f), respectively. The

IPF map of β phase for the through- β -transus processed microstructure is given in Fig. 7(g), in which β grain boundaries are delineated by white broken lines. The grain boundary α phase were indicated by black and yellow arrows, in the IPF maps and image quality or grain boundary maps, respectively.

In the β annealed bi-lamellar microstructure (Fig. 7(a) and (b)), a long and continuous grain boundary α phase ($\sim 400 \mu\text{m}$) with the same crystallographic orientation was observed along a straight β grain boundary. Consequently, only limited number of colonies formed in the β grains, resulting in a substantially large colony size. This is consistent with other studies on β annealed microstructures in $\alpha+\beta$ titanium alloys [21–24]. In contrast, in the β processed bi-lamellar microstructure (Fig. 7(c) and (d)), the β grain boundary became winded due to the hot deformation in β single-phase region. It was believed that the strain energy provided in the present process was not sufficient to induce dynamic recrystallization of β phase due to the high diffusivity of BCC structure especially in the β single-phase region, so that only dynamic recovery of β phase occurred during the β processing [26–28]. Thanks to the resultant curvature of β grain boundary, the length of grain boundary α phase formed during subsequent cooling became much shorter ($\sim 80 \mu\text{m}$) than that in the β annealed bi-lamellar microstructure. More importantly, the grain boundary α phase formed along segments of the winded β grain boundary had different crystallographic orientations. As a result, more colonies could nucleate from these grain boundary α segments with different crystallographic orientations, which eventually resulted in the smaller colony size. In fact, one can clearly see that many colonies in Fig. 7(c) have the same color (crystallographic orientation) as adjacent grain boundary α . However, there was a limitation for winding β grain boundaries due to the fast recovery of β phase at high temperatures, so that the colony size stayed in a similar value even though the compression strain increased over 1.2. In the through- β -transus processed lamellar microstructure (Fig. 7(e), (f) and (g)), the size (length) of the grain boundary α phase became even smaller ($\sim 8 \mu\text{m}$). Meanwhile, the distribution of the grain boundary α phase also changed from continuous ones in the β annealed and the β processed microstructures into discontinuous one in the through- β -transus processed microstructure indicated by the black and yellow arrows in Fig. 7(e) and (f). Such fine and discontinuous grain boundary α phase in the through- β -transus processed microstructure was attributed to the deformation during the early stage of cooling process across the β transus temperature. When the temperature decreased below the β transus temperature, newly formed grain boundary α phase along β grain boundaries were concurrently deformed. This would lead to the different crystal rotations within each grain boundary α phase and the formation of LAGBs and HAGBs between domains differently rotated. Each domains of grain boundary α phase subdivided tended to have more equiaxed morphologies at high temperatures for reducing the boundary energy. In addition, subsequent deformation at lower temperature may induce temperature rise, leading to reverse transformation of grain boundary α phase to β phase in part. Such a reverse transformation would happen preferentially at LAGBs/HAGBs introduced by the subsequent deformation, and make the grain boundary α phase discontinuous. In such a way, grain boundary α phase with a much smaller size and discontinuous distribution could be achieved in the through- β -transus processed microstructure, which led to a substantially refined colony size (Fig. 7(e)).

4.2. Deformation behaviors of traditional lamellar microstructure

In the lamellar microstructure, the yield and tensile strengths gradually increased with decreasing the colony size while the total elongation remained nearly the same. In our previous study on the mechanical properties of lamellar and bi-lamellar microstructures in Ti–6Al–4V alloy [20], the deformation behavior of lamellar microstructure has been briefly discussed. In this study, to discuss the deformation mechanism of lamellar microstructure more deeply, a lamellar microstructure with a colony of 60 μm was tensile deformed by a plastic strain of 4.0%.

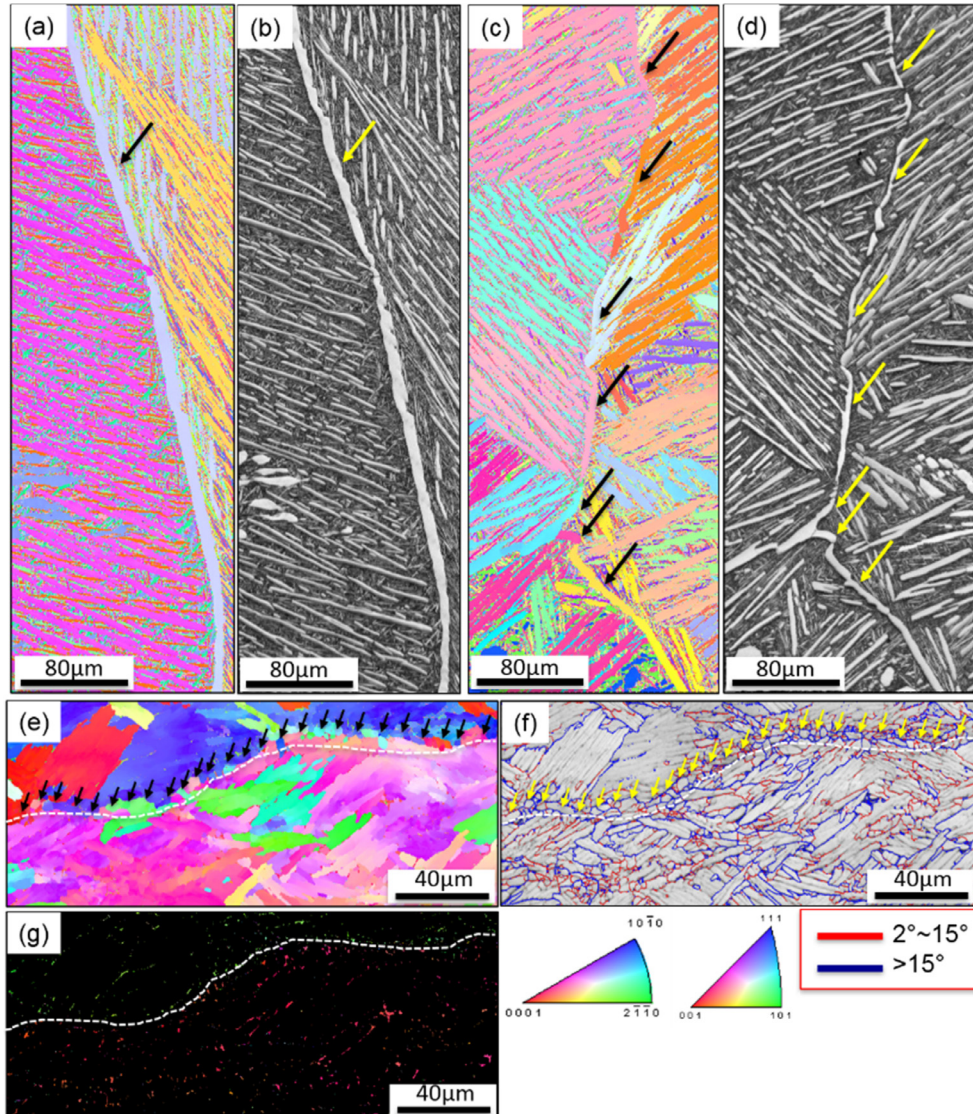
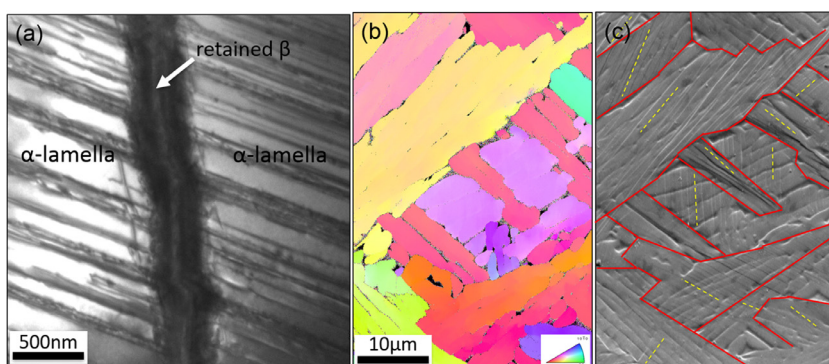


Fig. 7. EBSD characterization of the β annealed bi-lamellar microstructure (a, b), the β processed bi-lamellar microstructure by strain of 1.2 (c, d), and the through- β -transus processed lamellar microstructure (e-g). EBSD IPF maps of α phase in the microstructures are shown in (a, c and e), and corresponding image quality as well as grain boundary maps (blue: HAGBs, red: LAGBs) are shown in (b, d and f). In the IPF maps (a, c, e) and image quality or grain boundary maps (b, d, f), grain boundary α phase is marked by black and yellow arrows, respectively. The IPF map of β phase in the through- β -transus processed microstructure is given in (g), in which β grain boundaries are delineated by white broken lines. The compression axis is parallel to the longitudinal axis of all three microstructures. Long and continuous grain boundary α phase, short and continuous grain boundary α phase, and discontinuous grain boundary α phase were observed in the β annealed, β processed and through- β -transus processed microstructures, respectively.



In the typical TEM image showing a deformed lamellar microstructure (Fig. 8(a) [20]), two coarse α lamellae sandwich a thin retained β . Planar dislocation slip bands were observed in the α lamellae on both sides of the retained β . The slip bands in two α lamellae were parallel and seemed continuous, indicating that the planar dislocation slip easily penetrated the thin retained β to propagate into the next α lamella. In Ti-6Al-4V alloy, β to α phase transformation follows the Burgers orientation relationship (OR), $\{0001\}_{\alpha} // \{110\}_{\beta}$ and $<11-20>_{\alpha} // <1-11>_{\beta}$ [9]. It has been believed in previous studies that the α/β interface

Fig. 8. TEM image (a) of lamellar microstructure after tensile deformation by a plastic strain of 4.0% [20]. Long and parallel dislocation slip bands were observed inside the α lamellae on both sides of the thin retained β . EBSD IPF map of α phase (b) and corresponding SEM image (c) of the lamellar microstructure with an average colony size of 60 μm after tensile deformation by a plastic strain of 4.0%. The colony boundaries identified from the IPF maps (b) were delineated by red lines in (c). Slip line directions in α lamellae within each colony was indicated by yellow broken lines in (c).

maintaining Burgers orientation relationship in Ti-6Al-4V is semi-coherent, which facilitates dislocations passing through [10-16]. The effective slip length in the lamellar microstructure is considered to be the colony size, which is typically hundreds of microns. Such an easy penetration of dislocations through retained β and α lamellae can explain the low yield strength of the lamellar microstructures (Fig. 6(a)).

For a larger-scaled microstructure characterization over several different colonies of the lamellar microstructure, pre-polished surfaces of the tensile specimen were directly observed by EBSD for analyzing slip

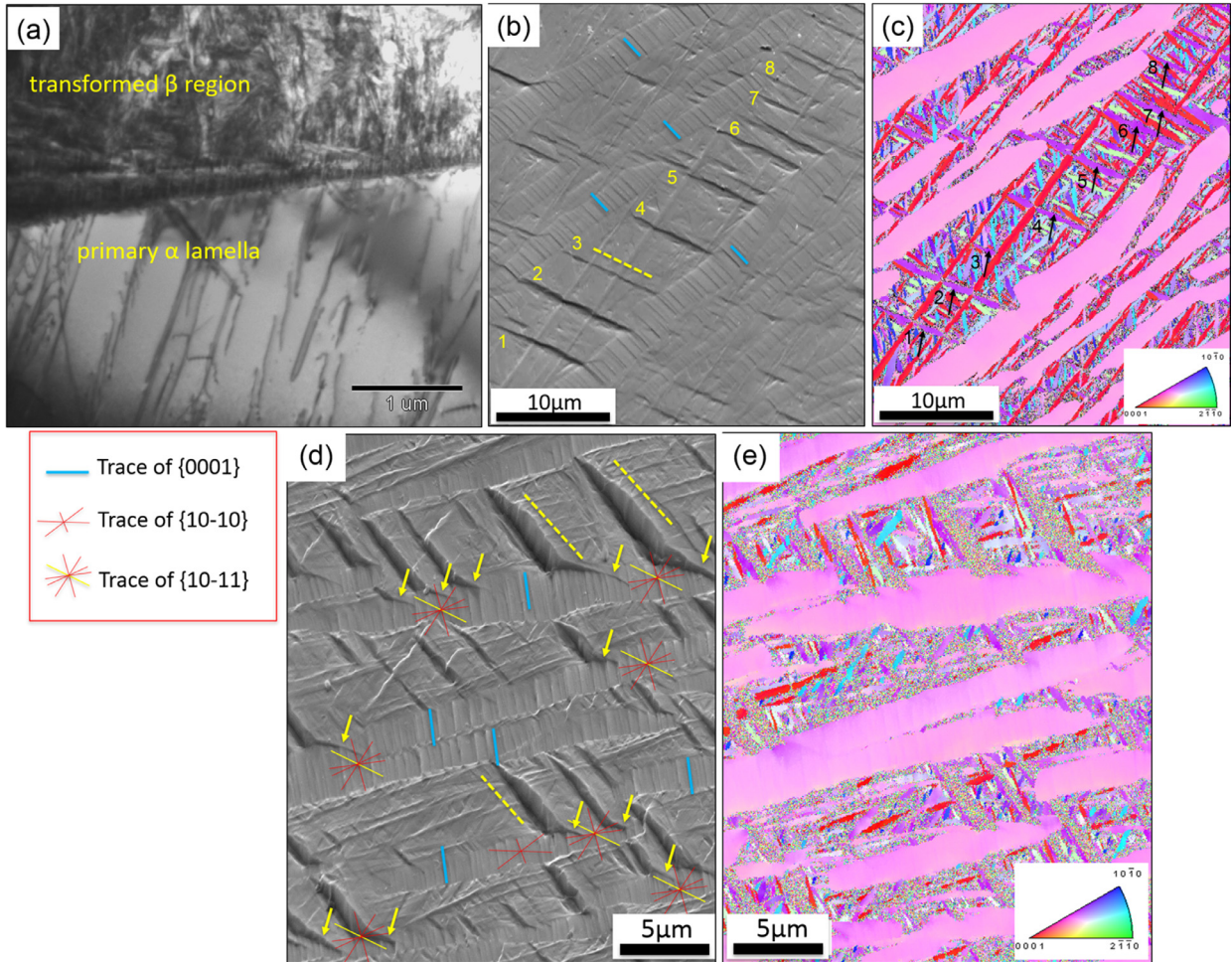


Fig. 9. Typical TEM image (a) of the bi-lamellar microstructure after tensile deformation by a plastic strain of 4.0%, in which dislocations inside the primary α lamellae were blocked at the interface between the primary α lamellae and the transformed β region. SEM and EBSD images of the bi-lamellar microstructure (with an equivalent colony size of 60 μm) after tensile deformation by plastic strains of 4.0% (b, c) and 10.0% (d, e). SEM images ((b), (d)) of the samples with electro-polished surface showed slip traces inside primary α lamellae and micro-shear bands (b), as well as micro-cracks (d) in transformed β regions after the tensile deformation. Slip lines and micro-shear bands/micro-cracks were indicated by blue solid lines and yellow broken lines, respectively. EBSD IPF maps ((c), (e)) of α phase for the same area were also shown. The micro-shear bands (c) tended to form along some secondary α lamellae (indicated by black arrows in (c)) having a specific orientation and direction. The micro-shear bands induced micro-cracks at a plastic strain of 10%, propagated to the neighboring primary α lamellae (indicated by yellow arrows in (d)) parallel to a {10-11} direction of the primary α lamellae (indicated by the yellow {10-11} plane trace).

line crystallographically. A typical EBSD IPF map of α phase and corresponding SEM image are shown in Fig. 8(b) and (c), respectively. The colony boundaries identified from the IPF map (Fig. 8(b)) were delineated by red lines in the SEM image (Fig. 8(c)). Slip lines within each colony could be easily identified in the SEM image and were indicated by yellow broken lines (Fig. 8(c)). It was clearly shown that each colony has a specific direction of the slip lines depending on its crystallographic orientation. The slip lines within one colony could hardly propagate into adjacent colonies. This indicated that the effective slip length in the lamellar microstructure was the colony size and the colony boundaries acted as strong obstacles against dislocations slips. Analogous to the Hall-Petch relationship of the equiaxed microstructures in which the yield strength increased with decreasing the average grain size [29–32], the increase in the yield strength with colony refinement observed in the lamellar microstructure is quite reasonable. In the equiaxed microstructures, the increase of the yield strength with grain refinement was usually accompanied by a loss of tensile ductility, especially when the grain size was reduced to several microns [29–32], which had been explained by the Considère plastic instability criterion. Nevertheless, in the present study, even the smallest colony size (60 μm) obtained in the lamellar microstructure was far above the fine grain sizes for which

significant loss in tensile ductility has been typically found [29–32]. That is, the relatively ‘coarse’ colony sizes (substantial grain sizes) in the lamellar microstructures could possibly explain the unchanged total elongation regardless of the colony size.

4.3. Achieving strength/ductility synergy in bi-lamellar microstructure

The bi-lamellar microstructures generally possessed higher yield and tensile strengths than the lamellar microstructures. In addition, unlike the case of the lamellar microstructures, the yield and tensile strengths of the bi-lamellar microstructures were independent of the colony size, however, the total elongation significantly increased with decreasing the colony size. A combination of high strength (~1100 MPa) and good ductility (~18.6%) can be achieved in the bi-lamellar microstructure with the smallest colony size (~60 μm). In order to explain the delayed tensile fracture in the bi-lamellar microstructure with a smaller colony size, the bi-lamellar microstructure with a colony size of 60 μm were tensile deformed by plastic strains of 4.0% (Fig. 9(a–c)) and 10.0% (Fig. 9(d and e)). A typical TEM image of the bi-lamellar microstructure after 4.0% tensile deformation is shown in Fig. 9(a). In sharp contrast to the case found in the deformed lamellar microstructure, dislocations in the

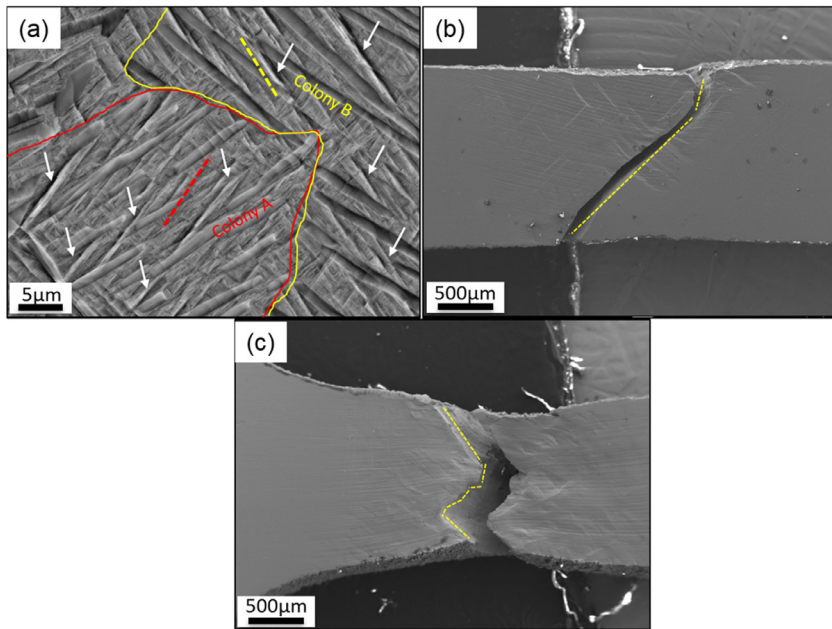


Fig. 10. SEM characterization of the specimens with bi-lamellar microstructures after tensile fracture. (a) Different directions of micro-shear bands (indicated by red and yellow broken lines) were found in two different colonies (marked as colony A and B). Colony boundaries of A and B were delineated by red and yellow lines, respectively. Some of the micro-shear bands were indicated by white arrows in the figure. (b) Macroscopic SEM image showing the tensile fracture of the bi-lamellar microstructure with a colony size of 280 μm . (c) Macroscopic SEM image showing the tensile fracture of the bi-lamellar microstructure with a colony size of 60 μm . The boundaries of the fracture surfaces were delineated by yellow broken lines in (b) and (c).

primary α lamellae were stopped at interfaces between primary α lamellae and transformed β regions in the bi-lamellar microstructure. Due to the large numbers of secondary α lamellae with various orientations as well as the α/β interfaces, dislocations activated in primary α lamellae could not easily pass through the transformed β regions. Therefore, dislocations piled up in primary α lamellae at interfaces with transformed β regions, and the piled-up dislocations provided additional strengthening by imposing back stress resisting the movement of following dislocations. The effective slip length in the bi-lamellar microstructure was, therefore, considered to be comparable to the thickness of primary α lamellae, which was only several microns and much smaller than the colony size. Such a situation explains the higher yield strength of the bi-lamellar microstructures than that of the lamellar microstructures.

In TEM, however, the deformation behavior of the transformed β regions could not be characterized. To solve this problem, SEM and EBSD characterizations were also carried out on the tensile deformed specimens with pre-polished surfaces. After tensile deformation by a plastic strain of 4.0%, slip lines (indicated by blue lines in Fig. 9(b)) frequently observed inside primary α lamellae were confirmed to belong to $\{0002\}<11\bar{2}0>$ basal slip, according to the slip line analysis using EBSD. Inside the transformed β regions, on the other hand, micro-shear bands (indicated by yellow broken lines) were typically observed instead of slip lines. As has been shown in Fig. 9(a), dislocations activated in primary α lamellae could not easily pass through the transformed β regions, so that dislocations piled up in primary α lamellae at interfaces with transformed β regions, leading to stress concentrations at the interface. Therefore, micro-shear bands had to form across the transformed β regions in order to propagate plastic strain. This indicates that the deformation of transformed β regions is microscopically heterogeneous, with plastic strains localized within the micro-shear bands. By tracking and comparing the locations of eight specific micro-shear bands (marked as 1–8 in Fig. 9(b) and (c)), it was found that all the micro-shear bands within the transformed β region showed the same direction, which coincided with the direction of specific secondary α lamellae (the α lamellae with a purple color indicated by black arrows in Fig. 9(c)). Similar results were also found in other regions of the specimen. When the tensile strain increased to 10.0%, both slip lines inside the primary α lamellae and micro-shear bands inside the transformed β regions became intensified (Fig. 9(d and e)). In this case, slip lines inside the primary α lamellae (indicated by blue lines in Fig. 9(d)) were also confirmed to

correspond to $\{0002\}<11\bar{2}0>$ basal slip. Some of the micro-shear bands induced micro-cracks (indicated by yellow broken lines) and then propagated into the adjacent primary α lamellae (indicated by yellow arrows in Fig. 9(d)), along one of the $\{10\bar{1}1\}$ plane traces of the primary α lamellae.

The evolution of micro-cracks from micro-shear bands at a larger tensile strain suggested that the micro-shear bands running across transformed β regions played a critical role to determine tensile fracture of the bi-lamellar microstructure. It was found that a specific direction of micro-shear bands developed in each colony and the specific directions were generally different between different colonies having different crystallographic orientations. One example is shown in Fig. 10(a), in which the directions of micro-shear bands were indicated by red and yellow broken lines for the colony A and B, respectively. The macroscopic SEM images of fractured specimens having the bi-lamellar microstructures with colony sizes of 280 μm and 60 μm are shown in Fig. 10(b) and (c), respectively. Outlines of fracture surfaces were delineated by yellow broken lines. The fracture surface of the bi-lamellar microstructure with a large colony size (280 μm) was quite straight and flat (Fig. 10(b)), indicating an easy propagation of the main crack. For the bi-lamellar microstructure with a smaller colony size (60 μm), on the other hand, the fracture surface was detoured and a macroscopic necking of the tensile specimen was clearly observed (Fig. 10(c)). The characteristics shown in Fig. 10(c) well coincide with the larger tensile elongation of the bi-lamellar microstructures with the smaller colony sizes, and suggest higher resistance for crack propagation in the microstructure.

Putting all the experimental results together, a clear picture of deformation and fracture in the bi-lamellar microstructures with different colony sizes can be drawn, as schematically illustrated in Fig. 11. Regardless of the colony size, the main deformation mechanisms in primary α lamellae and transformed β regions in the bi-lamellar microstructure were dislocation slip and micro-shear bands, respectively. The dislocation slip initiated in primary α lamellae cannot easily propagate into adjacent transformed β regions due to the existence of secondary α lamellae with various orientations as well as a large number of interfaces between secondary α lamellae and retained β in the transformed β regions. Dislocation pile-ups in primary α lamellae at interfaces with transformed β region lead to the stress concentrations, which inevitably induce localized deformation inside the transformed β regions in the form of micro-shear bands. The micro-shear bands in each colony have

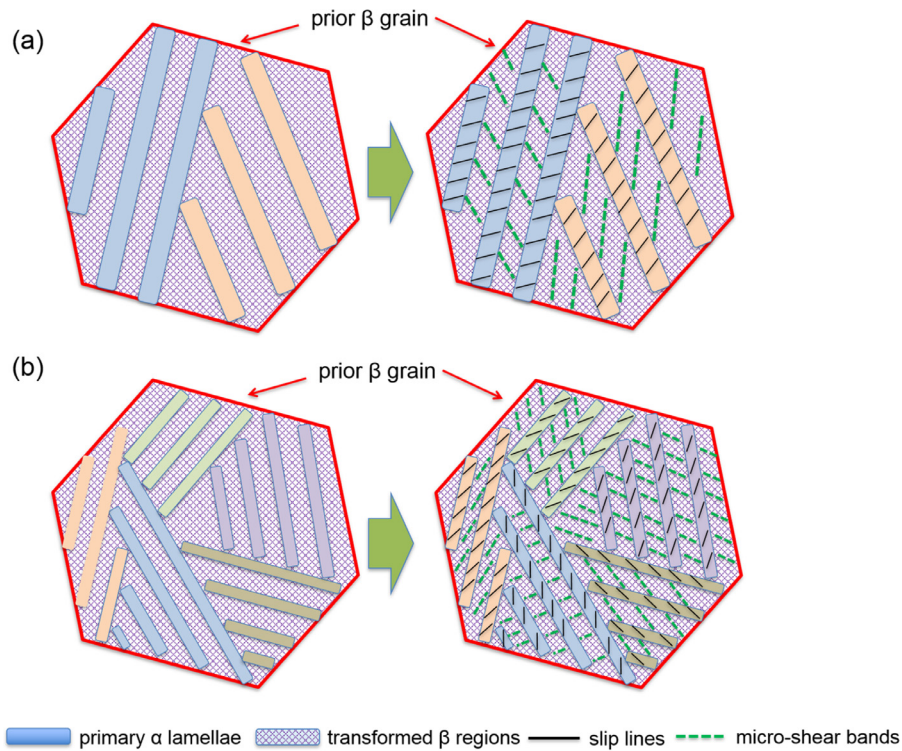


Fig. 11. Schematic illustrations showing the deformation behaviors in the bi-lamellar microstructures with larger (a) and smaller (b) colony sizes.

the specific direction, which is different in different colonies with different crystallographic orientations. With increasing the tensile deformation, the plastic strains localized in the micro-shear bands increase and eventually induce micro-cracks. Therefore, the variety of directions of the micro-shear bands as well as the micro-cracks plays a critical role in determining the fracture (the tensile elongation) of the bi-lamellar microstructures. In a bi-lamellar microstructure with a large colony size, the number of colonies is limited across the tensile specimen so that directions of micro-shear bands and micro-cracks are restricted. A large number of micro-cracks with the same direction would easily coalesce to form a large crack with larger stress concentration and propagate quickly across the tensile specimen. This leads to a limited total elongation (3.4%) as well as straight and flat fracture surface as well as the lack of necking in the tensile specimen having the bi-lamellar microstructure with a colony size of 280 μm (Fig. 10(b)). In contrast, in the bi-lamellar microstructure with a smaller colony size, much larger number of colonies are involved in the specimen, and the different colonies have different directions of micro-shear bands with different localized plastic strains. Macroscopic strain compatibility could be satisfied by the micro-shear bands with different directions in the bi-lamellar microstructure having the smaller colony size, which would delay the evolution of micro-cracks, their coalescence into the main crack and the propagation of the main crack. These can explain the much larger total elongation (18.6%), curved fracture surfaces, and larger necking of the tensile specimen found in the bi-lamellar microstructure with the smaller colony size of 60 μm .

5. Conclusions

In the present study, the colony size of both lamellar and bi-lamellar microstructures in Ti-6Al-4V alloy were successfully refined by a new thermomechanical process (the through- β -transus processing). The mechanisms of colony refinement were discussed with an emphasis paid on orientations and morphologies of grain boundary α phase. Furthermore, the mechanical properties of both microstructures with different colony sizes were systematically evaluated and the deformation

mechanisms were clarified in detail. The following conclusions could be drawn:

- (1) In the β processing method, the colony size gradually decreased with decreasing the hot-compression strain, resulting in the minimum colony size of 130 μm after a compression strain of 1.2. The colony size was further refined by the newly proposed through- β -transus processing, by which the smallest colony size of 60 μm was realized. In both methods, the colony refinement was attributed to the increased number of orientations and the change in morphologies of grain boundary α phase, which acted as nucleation site for subsequent formation of colony structures.
- (2) When the lamellar microstructures were intercritically annealed in $\alpha+\beta$ two-phase region and cooled at relatively high cooling rate, bi-lamellar microstructures comprised of primary α lamellae and transformed β regions were obtained. The colony sizes of the starting lamellar microstructures were maintained in the bi-lamellar microstructures.
- (3) The change of mechanical properties with the colony refinement showed different tendencies between the lamellar and bi-lamellar microstructures. In the lamellar microstructures, the tensile strength slightly increased with decreasing the colony size, while the total elongation remained almost unchanged. In the bi-lamellar microstructures, on the other hand, the total elongation fairly increased with decreasing the colony size, maintaining the high strength regardless of the colony size.
- (4) In the lamellar microstructures, colony boundaries having high-angle misorientations acted as barriers against dislocation slip, which resulted in the increase in the strength with the colony refinement. In the bi-lamellar microstructures, dislocation slips in primary α lamellae were hard to propagate into adjacent transformed β regions, and micro-shear bands formed in the transformed β regions played a critical role in determining deformation and fracture of the specimens. The variety of directions of the micro-shear bands in different colonies satisfied macroscopic compatibility of plastic deformation, which led to the larger

tensile elongation of the bi-lamellar microstructure with the smaller colony size.

Declaration of Competing Interest

The authors declare that they have no known competing financial interests or personal relationships that could have appeared to influence the work reported in this paper.

Acknowledgment

The authors are grateful to the financial supports from the Cross-ministerial Strategic Innovation Promotion Program (SIP) supported by the Cabinet Office of Japanese Government and the Elements Strategy Initiative for Structural Materials (ESISM) in Kyoto University supported by the [Ministry of Education, Culture, Sports, Science and Technology \(MEXT\)](#), Japan.

References

- [1] D. Banerjee, J.C. Williams, Perspectives on titanium science and technology, *Acta Mater.* 61 (2013) 844–879.
- [2] G. Lutjering, J.C. Williams, Titanium, Springer, 2003.
- [3] G. Lutjering, Influence of processing on microstructure and mechanical properties of $\alpha+\beta$ titanium alloys, *Mater. Sci. Eng. A* 243 (1998) 32–45.
- [4] S.L. Semiatin, V. Seetharaman, I. Weiss, The thermomechanical processing of alpha/beta titanium alloys, *JOM* 49 (1997) 33–39.
- [5] S.L. Semiatin, T.R. Bieler, The effect of alpha platelet thickness on plastic flow during hot working of Ti-6Al-4V with a transformed microstructure, *Acta Mater.* 49 (2001) 3565–3573.
- [6] S.L. Semiatin, V. Seetharaman, I. Weiss, Flow behavior and globularization kinetics during hot working of Ti-6Al-4V with a colony alpha microstructure, *Mater. Sci. Eng. A* 263 (1999) 257–271.
- [7] E.B. Shell, S.L. Semiatin, Effect of Initial Microstructure on Plastic Flow and Dynamic Globularization During Hot Working of Ti-6Al-4V, *30A* (1999) 3219–3229.
- [8] Y. Ito, S. Murakami, N. Tsuji, SEM/EBSD analysis on globularization behavior of lamellar microstructure in Ti-6Al-4V during hot deformation and annealing, *Metall. Mater. Trans. 48A* (2017) 4237–4246.
- [9] W.G. Burgers, On the process of transition of the cubic-body-centered modification into the hexagonal-close-packed modification of zirconium, *Physica* 1 (1934) 561–586.
- [10] S. Zherebtsov, G. Salishchev, S.L. Semiatin, Loss of coherency of the alpha/beta interface boundary in titanium alloys during deformation, *Philos. Mag. Lett.* 90 (2010) 903–914.
- [11] M. Cabibbo, S. Zherebtsov, S. Mironov, Loss of coherency and interface alpha/beta angular deviation from the Burgers orientation relationship in a Ti-6Al-4V alloy compressed at 800 °C, *J. Mater. Sci.* 48 (2013) 1100–1110.
- [12] S. Suri, G.B. Viswanathan, T. Neeraj, D.H. Hou, M.J. Mills, Room temperature deformation and mechanisms of slip transmission in orientated single-colony crystals of an α/β titanium alloy, *Acta Mater.* 47 (1999) 1019–1034.
- [13] D. He, J.C. Zhu, S. Zaeferer, D. Raabe, Effect of retained beta layer on slip transmission in Ti-6Al-2Zr-1Mo-1V near alpha titanium alloy during tensile deformation at room temperature, *Mater. Des.* 56 (2014) 937–942.
- [14] S. Suri, G.B. Viswanathan, T. Neeraj, D.H. Hou, M.J. Mills, Room temperature deformation and mechanisms of slip transmission in orientated single-colony crystals of an α/β titanium alloy, *Acta Mater.* 47 (1999) 1019–1034.
- [15] M.F. Savage, J. Tatajovich, M.J. Mills, Anisotropy in the room-temperature deformation of α/β colonies in titanium alloys: role of the α/β interface, *Philos. Mag.* 84 (2004) 1127–1134.
- [16] M.F. Savage, J. Tatajovich, M. Zupan, K.J. Hemker, M.J. Mills, Deformation mechanisms and microtensile behavior of single colony Ti-6242Si, *Mater. Sci. Eng. A* 319–321 (2001) 398–403.
- [17] G. Wegmann, J. Albrecht, G. Lutjering, et al., Microstructure and mechanical properties of titanium castings, *Z. Metallkd.* 88 (1997) 764–773.
- [18] L. Zhao, N. Park, Y. Tian, A. Shibata, N. Tsuji, Combination of dynamic transformation and dynamic recrystallization for realizing ultrafine-grained steels with superior mechanical properties, *Sci. Rep.* 6 (2016) 39127–39136.
- [19] Y. Chong, T. Bhattacharjee, M.-H. Park, A. Shibata, N. Tsuji, Factors determining room temperature mechanical properties of bimodal microstructures in Ti-6Al-4V alloy, *Mater. Sci. Eng. A* 730 (2018) 217–222.
- [20] Y. Chong, T. Bhattacharjee, N. Tsuji, Bi-lamellar microstructure in Ti-6Al-4V: microstructure evolution and mechanical properties, *Mater. Sci. Eng. A* 762 (2019) 138077.
- [21] N. Stanford, P.S. Bate, Crystallographic variant selection in Ti-6Al-4V, *Acta Mater.* 52 (2004) 5215–5224.
- [22] D. Bhattacharyya, G.B. Viswanathan, H.L. Fraser, Crystallographic and morphological relationships between β phase and the Widmanstatten and allotriomorphic α phase at special and special β grain boundaries in an α/β titanium alloy, *Acta Mater.* 55 (2007) 6765–6778.
- [23] E. Lee, R. Banerjee, S. Kar, et al., Selection of α variants during microstructural evolution in α/β titanium alloys, *Philos. Mag.* 87 (2007) 3615–3627.
- [24] D. Bhattacharyya, G.B. Viswanathan, R. Denkenberger, et al., The role of crystallographic and geometrical relationships between α and β phases in an α/β titanium alloy, *Acta Mater.* 51 (2003) 4679–4691.
- [25] Y. Chong, T. Bhattacharjee, Y.H. Yi, A. Shibata, N. Tsuji, Mechanical properties of fully martensite microstructure in Ti-6Al-4V alloy transformed from refined beta grains obtained by rapid heat treatment (RHT), *Scr. Mater.* 138 (2017) 66–70.
- [26] T. Furuhara, B. Poorganji, H. Abe, T. Maki, Dynamic recovery and recrystallization in titanium alloys by hot deformation, *JOM* 59 (2007) 64–67.
- [27] Y.C. Zhu, W.D. Zeng, F.F. Yu, Y. Sun, Y.F. Han, Y.G. Zhou, Characterization of hot deformation behavior of as-cast TC21 titanium alloy using processing map, *Mater. Sci. Eng. A* 528 (2011) 1757–1763.
- [28] Y.C. Zhu, W.D. Zeng, J.L. Liu, Y.Q. Zhao, Y.G. Zhou, H.Q. Yu, Effect of processing parameters on the hot deformation behavior of as-cast TC21 titanium alloy, *Mater. Des.* 33 (2012) 264–272.
- [29] N. Tsuji, N. Kamikawa, R. Ueji, N. Takata, H. Koyama, D. Terada, Ultrafine grained steels managing both strength and ductility, *ISIJ Int.* 48 (2008) 1114–1121.
- [30] N. Tsuji, Ultrafine grained steels managing both high strength and ductility, *J. Phys.* 165 (2009) 012010.
- [31] N. Tsuji, Y. Ito, Y. Saito, Y. Minamino, Strength and ductility of ultrafine grained aluminum and iron produced by ARB and annealing, *Scr. Mater.* 47 (2002) 893–899.
- [32] N. Tsuji, Y. Saito, S.H. Lee, Y. Minamino, ARB (Accumulative roll-bonding) and other new techniques to produce bulk ultrafine grained materials, *Adv. Eng. Mater.* 5 (2003) 338–344.